Quantitative in-cylinder fuel measurements in a heavy duty diesel engine using structured laser illumination planar imaging (SLIPI)

Sjoholm, Johan; Chartier, Clément; Kristensson, Elias; Berrocal, Edouard; Gallo, Yann; Richter, Mattias; Andersson, Öivind; Aldén, Marcus; Johansson, Bengt

DOI:
10.1299/jmsesdm.2012.8.500

2012

Document Version:
Publisher's PDF, also known as Version of record

Quantitative in-cylinder fuel measurements in a heavy duty diesel engine using Structured Laser Illumination Planar Imaging (SLIPI)

*Johan Sjöholm[a], Clément Chartier[b], Elias Kristensson[a], Edouard Berrocal[a], Yann Gallo[b], Mattias Richter[a], Öivind Andersson[b], Marcus Aldén[a], Bengt Johansson[b]

[a]*Division of Combustion Physics, Lund University, P.O. Box 118, SE-221 00 Lund, Sweden*
[b]*Division of Combustion Engines, Lund University, P.O. Box 118, SE-221 00 Lund, Sweden*

Key Words: SLIPI, quantitative LIF, fuel-jet, heavy duty diesel engine, jet-wall interactions

ABSTRACT

Laser-induced fluorescence (LIF) for quantitative fuel concentration measurements in a combustion engine is a challenging task. Measuring close to the walls of the combustion chamber is even more challenging as both the incident laser light and the signal are strongly reflected on the walls of the combustion chamber. By using a new technique called Structured Laser Illumination Planar Imaging (SLIPI) such background effects, as well as unwanted multiply scattered light, can be suppressed allowing for higher measurement accuracy. In this article we demonstrate, for the first time, the feasibility of the SLIPI technique for gas phase LIF and in-cylinder measurements. Results from regular LIF and SLIPI measurements are also compared. The measurements were made on a non-reacting fuel-jet with acetone as a fuel tracer in a heavy duty diesel engine (Scania D12). It is observed that the equivalence ratio measured by SLIPI in the free part of the jet is only two thirds of that measured by regular LIF during the early jet development.

INTRODUCTION

Global warming, increasing oil prices and stringent emission legislations stress the importance of clean diesel combustion with high efficiency. A deeper understanding of the actual fuel-jet may make it easier to reach emissions targets with maintained efficiency.

Optical diagnostics can contribute to this understanding and planar laser-induced fluorescence (LIF) is particularly useful for this purpose. However, there is still only limited information about the interaction between the fuel-jet and the combustion chamber wall since it is difficult to make accurate measurements close to the chamber walls.

Previous work in the engine used in this study has indicated that there is a surprisingly low correlation between the fuel-air ratio in the lift-off region and the engine out soot emissions [1]. Also, high speed LII measurements indicated that the early soot formation rate is independent of injection pressure [2]. A hypothesis is that the interaction between the jet and the bowl wall affects the air entrainment and soot oxidation in the downstream regions of the jet, which may have a dominant effect on the soot emissions.

To test this hypothesis, quantitative measurements of the equivalence ratio in the region where a fuel jet impinges on the bowl wall are required. One issue with such near-wall measurements are the strong reflections of the incident laser beam and the generated signal.

In this article a recently developed technique called Structured Laser Illumination Planar Imaging (SLIPI) [3] is tested and used for in-cylinder quantitative LIF. Due to its capability to filter out unwanted background contribution, the SLIPI technique is expected to provide measurements with higher accuracy compared to regular LIF, especially near the glass wall where the fuel-jet is impinging and where strong light reflections occur. A detailed comparison between SLIPI and regular LIF is also provided.

FUEL TRACER LIF

Planar LIF is a common way to measure the fuel distribution in a combustion engine. Most commercial fuels contain several species that fluoresce and that can be used for LIF measurements [4]. However, the extended distillation curve of these fuels together with the complicated temperature and pressure dependence of the combined signal (resulting from several simultaneously excited species) makes quantitative measurements extremely challenging.

Therefore, fuel tracer LIF, where a florescent tracer

is added to a non-fluorescing base fuel, is usually employed for quantitative measurements. This allows control of the tracer concentration, as well as pressure and temperature dependencies of the signal. A comprehensive summary of quantitative fuel tracer-LIF in practical combustion systems can be found in reference [5].

The detected LIF signal, I_{LIF}, can be expressed according to Eq. 1, following the notation in [6].

$$I_{LIF} = \frac{E}{h\nu}\frac{\chi_{tracer} P dV}{kT}\sigma(T,P,\chi,\nu)\eta(T,P,\chi,\nu)\frac{\Omega}{4\pi}\varepsilon \qquad (1)$$

Here E is the laser fluence [J/m^2], $h\nu$ is the laser's photon energy [J], χ_{tracer} is the mole fraction of the tracer [-], P is the pressure [Pa], dV is the excited volume imaged onto one pixel [m^3], T is the local temperature [K], σ is the absorption cross section [m^2], η is the fluorescence quantum yield [-], χ represent the local molecular composition [-] and ε is the efficiency of the detector and imaging optics including optical filters [-].

Using acetone as a tracer gives a very low pressure dependence on the combined absorption cross section and fluorescence quantum yield. Also, for non-reactive environment the variations in local gas composition are low, thus the P and χ dependencies can be removed. Assuming a constant collection angle, laser frequency, illuminated volume and detection efficiency gives Eq. 2

$$I_{LIF} = C\,E\frac{\chi_{tracer} P}{T}\sigma(T)\eta(T) = C\,E\chi_{tracer} P\,F(T) \qquad (2)$$

where C is a constant. Calculating the stoichiometric fuel-air ratio (assuming 21% O_2) gives together with the ideal gas law that $\chi_{tracer} = k\frac{\Phi}{52.4+\Phi} \approx k\,\Phi$. This final simplification gives a simple relation between the detected signal and the equivalence ratio (Φ)

$$\Phi = C'\frac{I_{LIF}}{E\cdot P\cdot F(T)} \qquad (3)$$

If E and P is are monitored during experiments with homogenous fuel distributions and varying inlet temperature and equivalence ratios, $F(T)$ and C' can be derived. For direct injection (DI) engines, this usually involves injecting fuel with an additional port fuel injector or injecting fuel very early in the cycle, giving ample time for mixing.

SLIPI

Quantitative fuel-tracer LIF measurements are difficult to perform in combustion engines. One important issue concerns the background subtraction of laser light that is scattered from the surrounding walls. Furthermore, multiply scattered LIF signals originating for the laser sheet and then scattered or originating from secondary fluorescence from walls etc. is not easily subtracted. The detection of these photons can lead to inaccuracy in the measurements.

By using SLIPI it is possible to remove these scattered light effects. SLIPI is based on laser sheets that are spatially modulated with a sinusoidal pattern, $E_{laser} = E_0\,(1+\sin(\omega x + p))$. The detected signal, I_1, from one modulated laser sheet is then

$$I_1 = I_B + I_S[1+\sin(\omega x + p_1)] \qquad (4)$$

where I_s is the amplitude of the modulation and I_B is the background offset arising e.g. from scattering and reflections. Combining three measurements with the phases, $p = 0°, 120°, 240°$ it is possible to reconstruct how the image would look without the modulation with Eq. 5.

$$I_{Reconstructed} = I_B + I_S = \frac{1}{3}(I_1 + I_2 + I_3) \qquad (5)$$

More significant, however, is that I_s can be retrieved from these three measurements according to Eq. 6 [7]. SLIPI can thus suppress the background and reveal the signal originating directly from the laser sheet.

$$I_s = \frac{\sqrt{2}}{3}\sqrt{[(I_1-I_2)^2 + (I_1-I_3)^2 + (I_2-I_3)^2]} \qquad (6)$$

In an ideal environment without distortions and noise, $I_{Reconstructed}$ and I_s are equal. However, when any background signal, e.g. from scattered or reflected light, is detected $I_{Reconstructed}$, containing a non-zero I_B, will differ from I_s.

In practical engine measurements, it is difficult to maintain the phase of the modulation at the exact desired value ($p = 0°, 120°, 240°$). The movement of the engine induces vibrations in the optical setup which causes the "lines" to shift. To overcome this issue, an new equation has been developed, based on the work published in [8]:

$$I_s = \frac{1}{2\left|\sin\left(\frac{p_1-p_3}{2}\right)\right|}\left|(I_3-I_1) + i\left\{\frac{I_1-I_2}{\tan\left(\frac{p_1-p_2}{2}\right)} - \frac{I_2-I_3}{\tan\left(\frac{p_2-p_3}{2}\right)}\right\}\right| \qquad (7)$$

Theoretically, it is possible to use any combination of phases in Eq. 7. However, due to the introduction of higher harmonics in the resulting image, I_s, the best results were experimentally found for phase differences between 100 and 140 degrees. Some other post-processing image corrections are necessary prior to the use of Eq. 6 or Eq. 7. These include correcting the three background levels to the mean level. These corrections and further details regarding the SLIPI technique can be found in [3].

EXPERIMENTAL SETUP

A sketch of the complete experimental setup is shown in Fig. 1(a). The laser (Continuum Powerlite DLS 9010) was operated in FHG mode generating 170 ±3 mJ of 266 nm radiation. The beam was first sent through an expanding telescope and an aperture in order to obtain a top hat beam profile before the grating. A square wave modulation was introduced using a Ronchi grating (reflective Chrome on fused silica substrate). To create the sinusoidal modulation frequency filtering of the beam was necessary as shown in Fig. 1 (b) and (c).

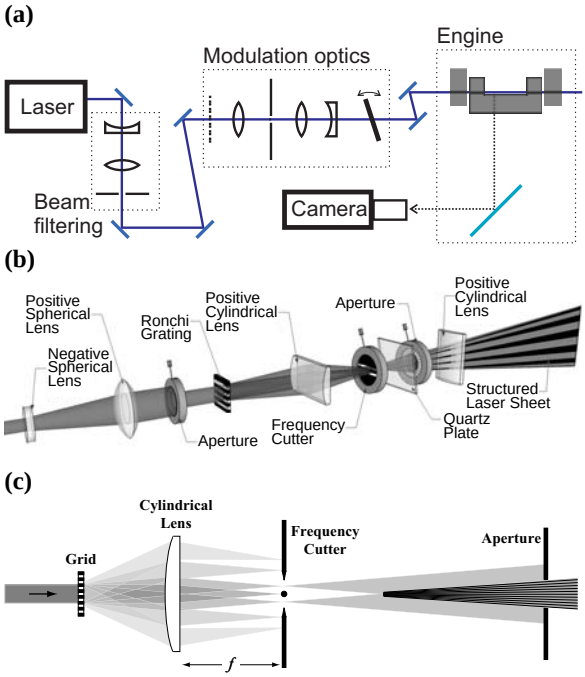

Figure 1: (a) Sketch of the experimental setup. (b) Detailed illustration of the optics employed for SLIPI measurements. (c) Description of the frequency filtering process used to create the sinusoidal modulation.

The beam was focused horizontally after the grating using an f = 200 mm cylindrical lens and the frequency filter was positioned in the focal plane. The frequency filter allowed only the first harmonic orders (± ω) from the grating to pass. A steel wire (∅ 0.4 mm) was used to reject lower frequencies (zero order) and two razor blades were used to block higher harmonics. The overlap and interference of the two first orders results in the formation a perfect sinusoidal pattern. This filtering process is shown in Fig.1 (c).

To horizontally shift the modulated laser sheet a 3 mm thick quartz plate (see Fig. 1 (a) and (b)) mounted on a rotation stage was used. By rotating the quartz plate to the correct angle, the desired modulation phase could be obtained. The three angles of the quartz plate, corresponding to the phases p = 0°, 120° and 240°, were selected so that the incident angles of the laser beam on the quartz plate were positioned symmetrical around the normal of the quartz plate to minimize optical distortions.

A cylindrical lens (f = 1000 mm) was used to focus the laser sheet in the vertical direction. The laser sheet thickness was ~1 mm across the entire measurement region. Finally, two dielectric mirrors and a translation stage were used to adjust the vertical position of the laser sheet prior to entering the optical engine (see Fig. 1(a)).

The engine used in this study was a Scania D12 heavy duty diesel engine, modified for single cylinder operation. Optical access was supplied from below through a Bowditch piston extension with a 45 degree mirror (UV enhanced aluminum) and through four side windows (28 mm wide and 22 mm high) in the combustion chamber liner. The fuel was isooctane with 10% acetone (by volume) and the inlet oxygen concentration was lowered to non-reacting conditions using an external EGR source.

The horizontal laser sheet entered the combustion chamber through one of the side windows in the liner. As the entire piston top was made from a single piece of quartz (glued to the piston extension) the laser sheet could enter the cylindrical piston bowl. A 3D sketch of the laser sheet and its position with respect to the quartz piston top and the fuel-jets can be seen in Fig 2. The laser sheet's vertical position was adjusted so that it matched the intersection point between the central axis of the fuel-jets and the bowl wall, about 2 mm from the bowl floor at top dead center (TDC). The laser sheet was initially 28 mm wide, corresponding to ~16 modulation waves, and slightly divergent in the combustion chamber.

The quartz piston top was found to fluoresce with 266 nm excitation (see Fig. 2). This fluorescence was spectrally and temporally overlapping with the acetone LIF signal and was used to measure the phase of the modulation even when no fuel tracer was present in the cylinder.

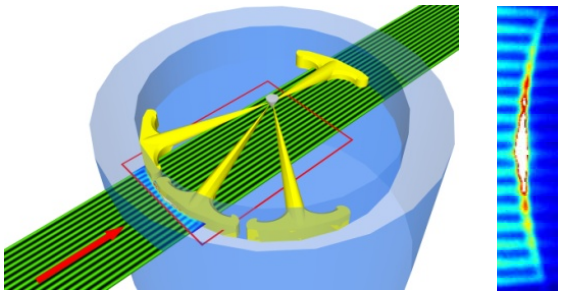

Figure 2: Left: Sketch of the quartz piston top (blue), structured laser sheet (green), fuel-jets (yellow) and the imaged area (red square). Right: image showing the fluorescence of the quartz piston.

Light was detected from below through the quartz piston top via the 45 degree mirror using a Princeton PI-MAX II ICCD camera (1024 × 1024 pixels) with a UV-acromatic lens (B. Halle, f = 100 mm, $f_{\#} = 2$). The pixels were binned 2 by 2 on chip (yielding 512 × 512 pixels) in order to increase the frame rate to >10 Hz. A long pass liquid filter before the camera lens (12 mm thick, N,N-dimetylformamid) was used to block elastically scattered laser light (a transmission curve can be found in reference [1]).

The imaging resolution was measured to f_{res} = 2.5 line pairs/mm using a test chart placed in the combustion chamber. Theoretically, a spatial modulation frequency close to half of the imaging resolution is optimal for structured illumination [8]. However, this is extremely challenging to work with experimentally and it is preferable to use a spatial frequency around $1/5 \cdot f_{res}$ [8] (0.5 line pairs/mm in this case). The final setup used here had a maximum modulation frequency of 0.46 line pairs/mm.

PROCEDURE AND CALIBRATION

Each SLIPI measurement followed the same routine. A run commenced with the engine being motored until intake and exhaust temperature stabilized (T_{in} = 398 K). Subsequently, fuel injection was started and images as well as pressure traces were recorded during 115 seconds, resulting in one SLIPI image. The engine was then stopped and the non-lubricated piston extension was allowed to cool down to a preset temperature while the intake manifold was kept at 398 K using the intake heater and a continuous gas flow through the manifold. During this time any cleaning of the optical parts in the engine was conducted. For each measurement, 350 images at each phase were averaged. Applying Eq. 7 to these three average images then resulted in one SLIPI image corresponding to 1050 engine cycles.

For comparison with the SLIPI measurements, single-shot regular LIF images were also collected. As the background level was found to vary with time, these images were collected by skip-firing the engine every second cycle and operating the laser and camera continuously. Thus, one background image was collected between each LIF image. 100 single-shot LIF images were collected for each measurement. Eq. 3 was used to extract the Φ values from the SLIPI (and LIF) images. In order to calculate *F(T)* and C' two calibrated port injectors 1 m upstream of the valves were used, guaranteeing a homogenous fuel distribution in the cylinder. The inlet system was constantly heated to avoid fuel condensation.

F(T) was calculated from measurements where the inlet temperature was varied (fixed amount of fuel) giving an in-cylinder temperature between 670 and 800 K (calculated from pressure traces) at the timing of the LIF measurement. C' was calculated from measurements with varying port injector duration (varying Φ). The correlation between Φ value and measured signal can be seen in Fig. 3 together with a calibration curve (following Eq. 3).

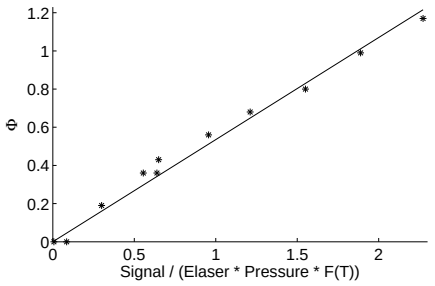

Figure 3: Φ as a function of signal strength divided by laser fluence, pressure and temperature function, F(T), and a calibration curve according to Eq. 3.

RESULTS AND DISCUSSIONS

Two raw data images with modulation can be seen in Fig. 4. The left image shows a case with port injection (homogenous Φ distribution). The slightly expanding laser sheet enters the combustion chamber from the left side where the fluorescence from the quartz piston top can be seen. The right image shows the signal at the same timing (4 CAD ATDC) with direct injection. Here the liquid parts of the sprays are visible to the right due to multiple scattering of light. The laser sheet only intersects the fuel-jets in the left part of the image due to the downward angle of the fuel-jets. Thus, no liquid fuel is expected in the laser sheet.

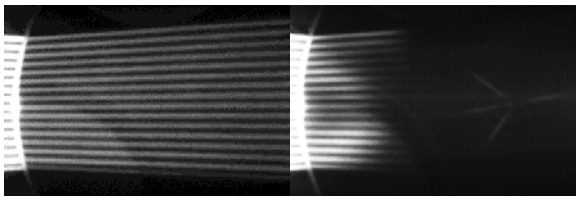

Figure 4: Raw data images (average of 350 cycles) with modulated laser sheets (I_1) for port injection (left) and direct injection (right) at 4 CAD ATDC.

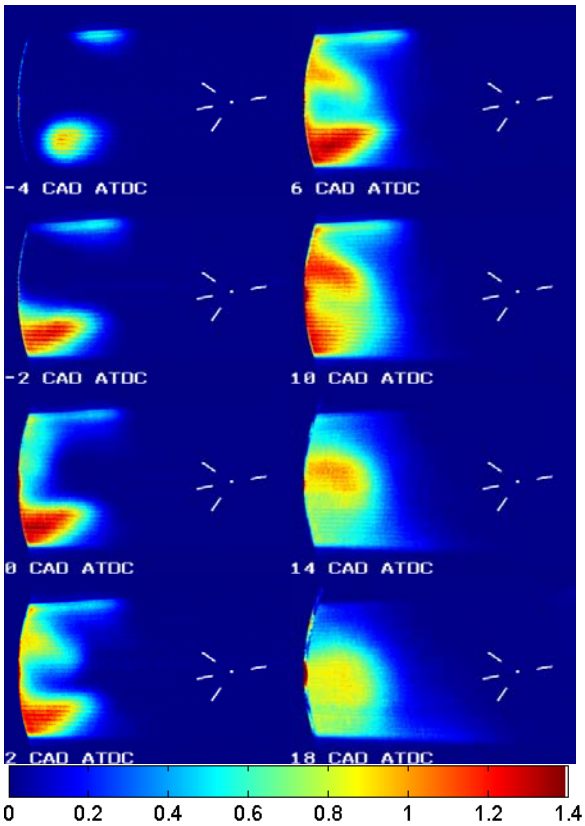

Figure 5: SLIPI images for varying timing (CAD ATDC). The color scale shows the Φ values.

Eight SLIPI images for acquisition timings between -4 and 18 CAD ATDC as indicated by the number in the lower left corner of each image can be seen in Fig. 5. The images are processed using Eq. 7 and rescaled to Φ values using Eq. 3. The white marks to the right in the images show the position and direction of the liquid fuel-jets.

The first image shows the free jet at -4 CAD ATDC before wall impingement. At -2 CAD ATDC the jet has impinged the bowl wall and at 2 CAD ATDC the

recirculation zone can be seen between the two fuel-jets. The recirculation zone expands towards the bowl center and is moved counterclockwise due to the swirling flow.

Actual SOI was at -7.5 CAD ATDC and actual EOI was at 7.7 ±0.1 CAD ATDC (appearance/disappearance of the liquid jets). The rapid air entrainment in the free jet (before wall impingement) after EOI can clearly be seen between 6 and 10 CAD ATDC.

Some residual stripes can be observed in the SLIPI images. These probably result from vibrations during the measurements. Note that the modulation frequency of the residuals is much higher than the original modulation frequency (shown in Fig. 4).

LIF – SLIPI COMPARISON

As a comparison to the SLIPI images, single-shot regular LIF images were also recorded (without modulation). Four examples can be seen Fig. 6 in order to illustrate the cycle to cycle variations in this case.

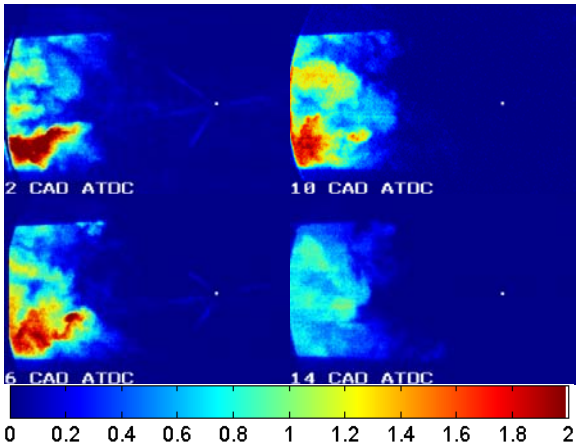

Figure 6: Single-shot regular LIF images for four timings. The color scale shows the Φ values.

Average LIF images, matching Fig. 5, can be seen in Fig. 7. The color scales in Fig. 5 – 7 show the local equivalence ratio in each pixel as indicated by the color bar at the bottom of each figure. Note that the color scale extends to Φ = 2 for the LIF images, as opposed to Φ = 1.4 for the SLIPI images. Each image in Fig. 7 is an average of 100 cycles. The liquid fuel-jets can be seen in Fig. 7 between -4 and 6 CAD ATDC as these scattering effects could not be removed with the background subtraction. The recirculation zone between the two jets is not as pronounced in Fig. 7 as in Fig 5. The LIF images also indicate overall higher Φ values compared the SLIPI images, especially in the free jet.

To further illustrate the differences between the Φ distributions measured by SLIPI and regular LIF, an evaluation path starting at the injector and following the mean trajectory of the jet was selected and analyzed. The path (5 pixels wide and 76.6 mm long) is illustrated by the white line in the top left image in Fig. 8.

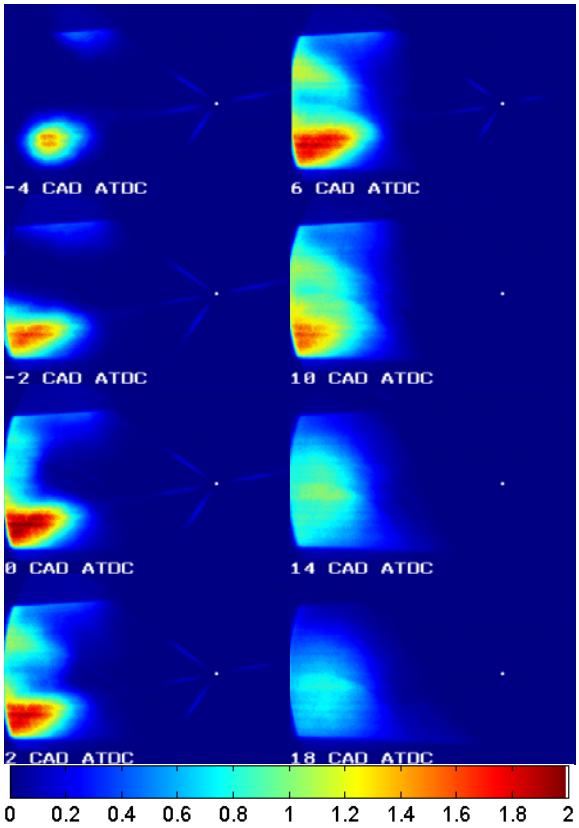

Figure 7: Average regular LIF images for varying timing (CAD ATDC). The color scale shows the Φ values

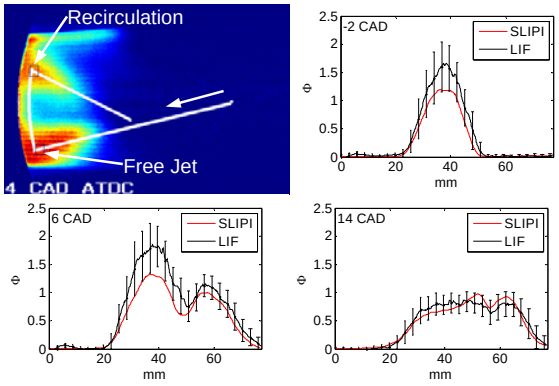

Figure 8: Φ values along the mean path of the jet (white line in the top left image) for -2, 6 and 14 CAD ATDC.

The resulting Φ values along the path for three different timings (-2, 6 and 14 CAD ATDC) are presented in Fig. 8 for both regular LIF (black curve, with the standard deviation shown by the error bars) and SLIPI (red curve).

These results show that regular LIF yields higher Φ values than SLIPI in the region of the free jet (<40 mm), but not in the recirculation region (~60 mm). In order to verify this observation, 14 successive SLIPI measurements were made with exactly the same settings at 4 CAD ATDC. Fig. 9 shows the resulting average curve with the corresponding standard deviation. It is seen that the standard deviation in Φ for the SLIPI

measurements remains relatively low, and that the average Φ values are in the same range as the ones shown in Fig.8. This confirms that the divergences observed in Fig.8 were not caused by experimental artifacts in the SLIPI measurement.

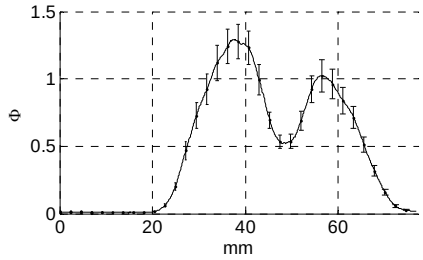

Figure 9: Average curve from 14 SLIPI measurements at 4 CAD ATDC corresponding to 14 700 individual cycles. The error bars indicate the standard deviation.

To further illustrate that SLIPI yields lower Φ values than regular LIF in the free jet, the average signal in two small regions (2,4 x 1.8 mm) close to the bowl wall were calculated. One region was positioned in the recirculation zone and one was placed in the free jet just upstream of the wall impingement (shown by the black squares in Fig. 8, top left). The resulting signal as a function of CAD ATDC for both LIF and SLIPI can be seen in Fig. 10. The two curves from the recirculation zone (dotted lines) overlap well with no significant difference. In the free jet, however, the LIF images indicate up to one third higher Φ values compared to the SLIPI images. After EOI at 7.7 CAD ATDC the difference decreases and similar Φ-values are measured.

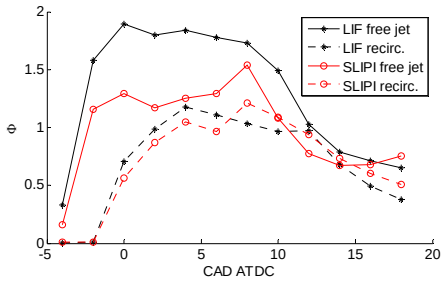

Figure 10: Φ in the recirculation zone and the impingement region of the free jet measured with LIF and SLIPI as a function of CAD ATDC.

The main advantage of SLIPI is the possibility to suppress complex background effects that cannot be suppressed using a standard background subtraction. Therefore, SLIPI provides more accurate results in scattering environments (e.g. removal of the signal from the liquid jets in Fig. 5) as well as near scattering surfaces (e.g. close to the walls) where the background signal can be so strong that it hinders the desired signal. SLIPI removes these effects and can thus measure more accurately closer to the wall.

Multiple scattering give rise to volumetric illumination. This tends to overestimate the LIF signal and is probably one of the causes behind the effects shown in Fig 10. This phenomenon is difficult to account for in regular LIF measurements. An increased multiple scattering in the free jet would increase the LIF signal as compared to the SLIPI signal where it would be removed. However, it is also possible that the thermal boundary layer is affected by the impact of the fuel-jet on the wall. This would create an inhomogeneous thermal gradient that would affect the incident modulation and lower the SLIPI signal. The exact causes for the differences between the LIF and SLIPI in the free-jet are difficult to determine precisely and further investigation are required to elucidate the observed phenomenon.

CONCLUSIONS

In this paper we demonstrate, for the first time, the feasibility of the SLIPI technique for gas phase LIF and for in-cylinder measurements in a heavy duty diesel engine. The regular LIF – SLIPI comparison shows a clear difference in the free jet, where higher equivalence ratios (up to one third higher) are measured with regular LIF. Such differences seem to be due to SLIPI suppressing multiply scattered signal which, with LIF, seems to lead to overestimated Φ-values. However, other complex effects such as inhomogeneous thermal gradients might also occur, providing further explanation of these differences. More work is required to determine whether the LIF measurements overestimate or the SLIPI measurements underestimate the equivalence ratio.

Acknowledgements The authors would like to acknowledge the Swedish Energy Agency for their support.

REFERENCES

[1] Aronsson, U., Chartier, C., Andersson, Ö., Egnell, R., Sjöholm, J., Richter, M. and Aldén, M., *SAE Technical Paper 2009-01-1357*, (2009).

[2] Sjöholm, J., Wellander, R., Bladh, H., Richter, M., Bengtsson, P.-E., Alden, M., Aronsson, U., Chartier, C., Andersson, O. and Johansson, B., *SAE Int. J. Engines*, 4(1), 1607-1622 (2011).

[3] Kristensson, E., in: *Ph.D. thesis in Combustion Physics*, Lund University: 2012.

[4] Fansler, T. D., French, D. T. and Drake, M. C., *SAE Technical Paper 950110*, (1995).

[5] Schulz, C. and Sick, V., *Progress in Energy and Combustion Science*, 31, (1), 75-121 (2005).

[6] Sahoo, D., Petersen, B. and Miles, P., *SAE Int. J. Engines* 4, (2), 2312-2325 (2011).

[7] Neil, M. A. A., Juskaitis, R. and Wilson, T., Opt. Lett., 22, 1905-1907 (1997).

[8] Cole, M. J., Siegel, J., Webb, S. E. D., Jones, R., Dowling, K., Dayl, M. J., Parsons-Karavassilis, D., French, P. M. W., M.J., L., Sucharov, L. O. D., Neil, M. A. A., Juskaitis, R. and Wilson, T., J. Microsc., 203, 246-257 (2000).